An anticlastogenic function for the Polycomb Group gene Bmi1

Jalila Chagraoui[a], Josée Hébert[a,b,c], Simon Girard[a], and Guy Sauvageau[a,b,c,1]

[a]Laboratory of Molecular Genetics of Hematopoietic Stem Cells, Institute for Research in Immunology and Cancer, Université de Montréal, Montréal, QC, Canada H3C 3J7; and [b]Division of Hematology, Department of Medicine and [c]Leukemia Cell Bank of Quebec, Maisonneuve-Rosemont Hospital, Montréal, QC, Canada H1T 2M4

Edited by Suzanne Cory, The Walter and Eliza Hall Institute, Melbourne, VI, Australia, and approved February 16, 2011 (received for review September 24, 2010)

***BMI1* is a key component of multiprotein Polycomb repression complex 1 (PRC1), and its disruption in mice induces severe aplastic anemia by early adulthood. The contributing mechanisms responsible for this phenotype remain elusive. Here we show that transformed human cell lines as well as primitive hematopoietic cells exhibit a high frequency of spontaneous chromosome breaks upon BMI1 depletion and are hypersensitive to genotoxic agents. Consistent with these observations, we found that BMI1 is recruited rapidly to DNA damage foci where it blocks transcriptional elongation. We also show that BMI1 contributes to homologous recombination DNA repair and is required for checkpoint recovery. Taken together, our results suggest that BMI1 is critical for the maintenance of chromosome integrity in both normal and transformed cells.**

The Polycomb group gene (PcG) *Bmi1* is known as a key determinant of normal and leukemic hematopoietic stem cell (HSC) function. In its absence HSCs fail to self-renew, leading to bone marrow failure and profound anemia in young mice. Although many functions have been ascribed to BMI1, the molecular mechanisms underlying its role in HSCs remain uncertain. In mouse and human fibroblasts, *Bmi1* genetically interacts with $p16^{ink4a}$ and/or $p19^{arf}$ to prevent senescence (1–4). BMI1 binds the loci together directly with other PcG proteins leading to changes in histone modifications compatible with gene repression (5, 6). Evidence suggests that the inactivation of *ink4a*/*arf* is not the sole mechanism by which BMI1 regulates HSC activity. In support of this evidence, $Bmi1^{-/-}$ leukemia cell lines lacking expression of $p16^{ink4a}$ and $p19^{arf}$ still require the ectopic expression of *Bmi1* to generate leukemia in vivo (7). Moreover, the demonstration that *Bmi1* genetically interacts with E4 transcription factor 1 (*E4f1*), an atypical p53 E3 ubiquitin ligase (8), to regulate the repopulating activity of HSCs in an INK4a/ARF-independent manner further substantiates this hypothesis (9).

Biochemical studies recently showed that the PcG protein ring finger protein 2 (RNF2) is an E3 ubiquitin ligase exhibiting monoubiquitination activity toward histone H2A. BMI1 has been proposed to protect RNF2 from degradation and to enhance its monoubiquitinating activity (10).

Several studies suggested that PcG proteins, including BMI1, have a role in the DNA damage response/repair process (11–13). Hong et al. (14) recently reported the immediate recruitment of the Polycomb repressive complex 2 (PRC2)-associated PHD finger protein 1 (PHF1) to double-strand breaks (DSB) following irradiation. PHF1 interacts directly with KU70/KU80 and RAD50 proteins, and its knockdown sensitizes cells to irradiation. Similarly, Rouleau et al. (15) showed that poly(ADP ribose)polymerase 3 (PARP-3), which interacts with proteins typically found at DSBs in the nonhomologous end-joining (NHEJ) pathways, is part of the PRC2 complex that includes enhancer of zeste homolog 2 (EZH2) and suppressor of zeste 12 homolog (SUZ12). Together these observations strongly suggest a role for the PRC2 in the NHEJ repair pathway.

Using RNAi, Bergink et al. (16) demonstrated that UV-induced H2A monoubiquitination is reduced in cells engineered to express low levels of the RNF2 PcG protein. Recently, the SUMO E3 ligase PcG gene *Pc2*, known to interact with BMI1 and RNF2 within Polycomb repression complex 1 (PRC1), has been shown to be essential for the sumoylation and nuclear localization of centrin 2 required in the nucleotide-excision repair process (17).

Two recent studies have linked *Bmi1* to oxidative metabolism. Chatoo et al. (18) reported that *Bmi1* prevents intracellular accumulation of reactive oxygen species (ROS) in neurons through repression of p53 pro-oxidant activity. Liu et al. (19) showed that *Bmi1* deficiency leads to increased expression of several genes involved in ROS homeostasis and mitochondrial function. They also demonstrated that the activation of ROS-mediated DNA damage response in *Bmi1*-deficient mice occurs in an *ink4a*/*arf*-independent manner. (19) Here, we build on these observations and show that BMI1 ensures the maintenance of chromosome integrity in both normal and transformed cells by promoting transcriptional repression at the lesions. We also document that the loss of Bmi1 recapitulates several phenotypes associated with genomic instability syndromes (i.e., cell-cycle defects, DNA damage sensitivity, and ROS accumulation) that often result in bone marrow failure, immunodeficiency, congenital abnormalities, and growth retardation.

Results

Correlation Between Survival of $Bmi1^{-/-}$ Mice and Activity of Long-Term Repopulating HSC. Deletion of *Bmi1* leads to axial skeleton patterning and hematopoietic defects, severe ataxia, and seizures. Although *Bmi1*-deficient mice survive after birth, about half of them die before the weaning period (3 wk old) (20). Mice that do survive the first days die within 4–10 wk. By simplifying young ataxic animals' access to water and nutrients, we were able to extend the median and maximum lifespan of *Bmi1*-deficient mice significantly, to 150 d (Fig. S1*A*), at which time a phenotype of very severe bone marrow failure was observed. Considering the 4- to 5-mo transition period typically associated with HSCs that show short- or intermediate-term versus long-term repopulation (LTR) potential (21), these data are consistent with the hypothesis that *Bmi1* deficiency is not compatible with the maintenance of LTR-HSC activity (Fig. S1*B*).

Cell-Cycle Progression Defect in $Bmi1^{-/-}$ HSCs. By conducting a series of genetic complementation studies (Fig. S1*C*), we showed that disruption of p53/pRb pathways (E6–E7), prevention of premature senescence (T-box 2, TBX2) (22) or reduction of ROS levels (*N*-acetyl cysteine, NAC) failed to restore the LTR activity of $Bmi1^{-/-}$ HSCs (Fig. S1 *D* and *E*). Although freshly isolated $Bmi1^{-/-}$ fetal liver cells can be fully rescued by *Bmi1* or

Author contributions: J.C. and G.S. designed research; J.C. performed research; J.H. and S.G. contributed new reagents/analytic tools; J.C., J.H., and S.G. analyzed data; and J.C. and G.S. wrote the paper.

The authors declare no conflict of interest.

This article is a PNAS Direct Submission.

[1]To whom correspondence should be addressed. E-mail: guy.sauvageau@umontreal.ca.

This article contains supporting information online at www.pnas.org/lookup/suppl/doi:10.1073/pnas.1014263108/-/DCSupplemental.

its ΔPEST mutant, it was impossible to rescue *Bmi1*$^{-/-}$ cells that were kept in culture for 2 d or more.

To gain further insights into this observation, we examined the cell-cycle status of primitive *Bmi1*$^{-/-}$ hematopoietic cells that were kept in culture under growth conditions that normally support fetal liver HSC activity (23). As shown in Fig. S1*F*, cultures initiated with these cells showed a significant increase of both cycling (fewer cells in G0) and apoptotic (subG1) cells compared with control HSCs. Strikingly, *Bmi1*$^{-/-}$ HSCs accumulated in G2 (Fig. S1*F*). This finding indicates that *Bmi1*-deficient fetal liver HSCs are exquisitely sensitive to ex vivo manipulation and are impaired irreversibly after a few days in culture. Overall, these data suggest that the severe phenotype observed in *Bmi1*$^{-/-}$ cells is likely to be the result of cumulative effects rather than being attributable only to deregulation of p53 or pRb pathways.

γ-H2AX Foci Formation in the Absence of BMI1. The multiple cell-cycle anomalies observed in cultured *Bmi1*$^{-/-}$ cells, together with the growing body of evidence linking PcG genes to DNA damage response, prompted us to investigate further the potential role for *BMI1* in this process.

We first performed a series of time-course experiments to characterize the appearance of DNA damage-induced γ-H2AX foci in murine embryonic fibroblasts (MEF) freshly isolated from wild-type or *Bmi1*$^{-/-}$ mice. As expected, in wild-type MEF, γ-H2AX^{+} foci could be detected as early as 5 min after ionizing radiation (T = 5 min) (Fig. 1*A*). The number of γ-H2AX^{+} foci per cell (Fig. 1*C*, white bars) as well as the percentage of positive cells (Fig. 1*D*, black line), increased markedly by 4 h after irradiation. Consistent with a normal DNA-repair process, the number of γ-H2AX foci returned to baseline levels when examined 24 h postirradiation (Fig. 1 *A*–*C*).

Strikingly, we observed a two- to threefold increase in the number of spontaneous γ-H2AX foci in *Bmi1*$^{-/-}$ versus wild-type MEF (Fig. 1*B Upper* and *D*). The early appearance (T = 5 min) of γ-H2AX foci was not affected by the absence of *Bmi1* (Fig. 1*B*). At 24 h postirradiation, however, we noted a fivefold increase in the proportion of cells with persistent γ-H2AX foci in *Bmi1*-deficient MEF as compared with wild-type (33 ± 5% vs. 6 ± 2%, respectively) (red box in in Fig. 1*B Bottom Right* and gray line in Fig. 1*D*).

S-G2/M Checkpoint Recovery Defect in *Bmi1* Mutant Cells. To test whether the presence of persistent γ-H2AX foci in *Bmi1*-deficient MEF is associated with a defect in checkpoint recovery, we performed BrdU pulse-chase experiments to label cells in S phase selectively at the time of camptothecin (CPT) treatment and to track their progression through the cell cycle after CPT removal. Importantly, we did not find obvious differences in cell-cycle distribution and kinetics between untreated wild-type and *Bmi1*-null cells (Fig. S2, compare panels in rows 1 and 2). As expected, CPT treatment delayed the progression from S to G2/M in wild-type cells (Fig. S2 *C1* and *C3*). By 12 h, most of these CPT-treated cells had moved into G2/M (Fig. S2*D3*), consistent with a checkpoint release of repaired wild-type cells. In contrast, *Bmi1*$^{-/-}$ cells failed to recover from CPT treatment, as shown by a prolonged arrest at the S-phase checkpoint (compare progression of *Bmi1*$^{-/-}$ cells in Fig. S2 *C4* and *D4* with that of wild-type cells in Fig. S2 *C3* and *D3*).

Spontaneous Chromosome Breaks in Cell Lines with Reduced *Bmi1* Levels. The persistence in checkpoint activation and γ-H2AX foci in *Bmi1*$^{-/-}$ cells along with the aplastic anemia phenotype suggested that BMI1 might be implicated in maintenance of chromosome integrity. To test this hypothesis, we first correlated the frequency of spontaneous chromosome breaks in two well-characterized human cell lines (HCT116 and 293T) in which BMI1 levels are acutely decreased by the use of shRNA vectors. To facilitate cytogenetic analysis, we used the HCT116 cell line, a human near-diploid colon carcinoma cell line with few well-known chromosomal abnormalities.

In both cell lines, *Bmi1* knockdown resulted in the formation of radial chromosome forms reminiscent of some chromosomal instability syndromes. We also observed an increase in the rate of spontaneous chromosome breaks in both *shBmi1*-transfected cell lines (arrows in Fig. S3*A*). HCT116 cells transfected with a control vector showed a maximum of two breaks per cell, with 84% of cells having no chromosome breaks (black bars in Fig. S3*B*). In contrast, *shBmi1*-transfected HCT116 cells were more susceptible to spontaneous chromosome breakage, with a maximum of 16 breaks per cell and with 56% of cells having more than two breaks (white bars). Similarly, although 62% of control 293T cells showed no break, 84% of *shBmi1*-transfected 293T cells displayed more than two breaks per cell (Fig. S3*B Right*). *shBmi1*-transfected 293T cells exhibited a much higher frequency of chromosome breakage than *shBmi1*-transfected HCT116 cells, with the number of breaks per cell exceeding 20 in 56% of the scored metaphases (Fig. S3*B*). Together these results link spontaneous chromosome breakage with reduction in BMI1 protein levels.

Loss of *Bmi1* Renders Cells Hypersentitive to Clastogenic Agents. To investigate if *Bmi1* impairment affects chromosome integrity upon DNA damage, we performed cytogenetic analysis of HCT116 and 293T cells engineered to express low levels of *Bmi1* and exposed to different clastogens. As shown in Fig. 2*A*, *Bmi1* knockdown resulted in a marked increase of CPT- and aphidicolin-(APH) induced chromosome breaks in both cell lines (red arrows).

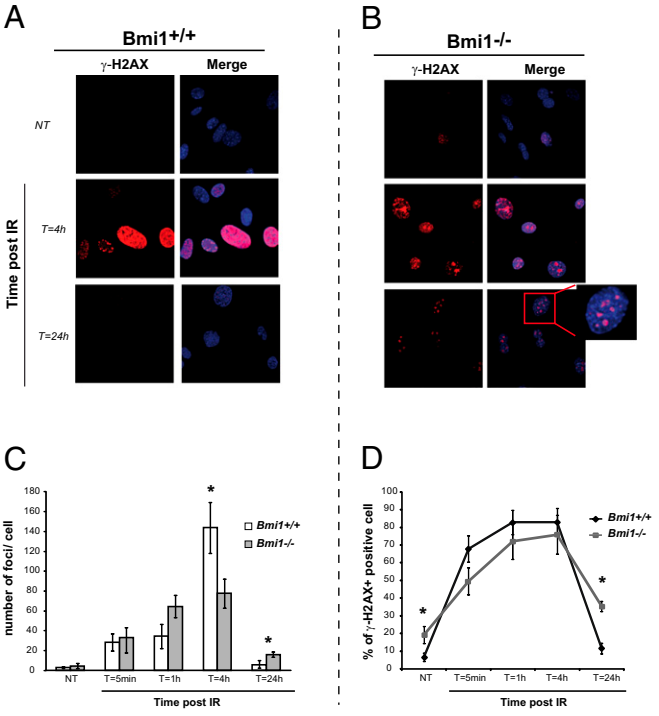

Fig. 1. Spatiotemporal dynamics of γ-H2AX^{+} foci formation in wild-type and Bmi1$^{-/-}$ MEF after irradiation. (*A*) *Bmi1*$^{+/+}$ MEF were untreated (NT) or irradiated at 10 Gy and incubated at 37 °C for the indicated recovery time. The cells were preextracted before fixation and immunostained for γ-H2AX (red) and DAPI (blue). Representative confocal images of six independent experiments are shown. (*B*) Bmi1$^{-/-}$ MEF (passage 2) were untreated (NT) or irradiated at 10 Gy and processed as in *A*. Representative confocal images from four independent experiments are shown. (*C*) Quantitative assessment of the number of γ-H2AX^{+} foci per cell in *Bmi1*$^{+/+}$ MEF (white bars) and *Bmi1*$^{-/-}$ MEF (gray bars). A minimum of 50 cells were scored for each time point. Values (mean ± SD) from three independent experiments are shown. *$P < 0.005$; Student *t* test. (*D*) Percentages of γ-H2AX^{+} cells in *Bmi1*$^{+/+}$ MEF (black line) and *Bmi1*$^{-/-}$ MEF (gray line). Values (mean ± SD) from three experiments are shown. *$P < 0.005$; Student *t* test.

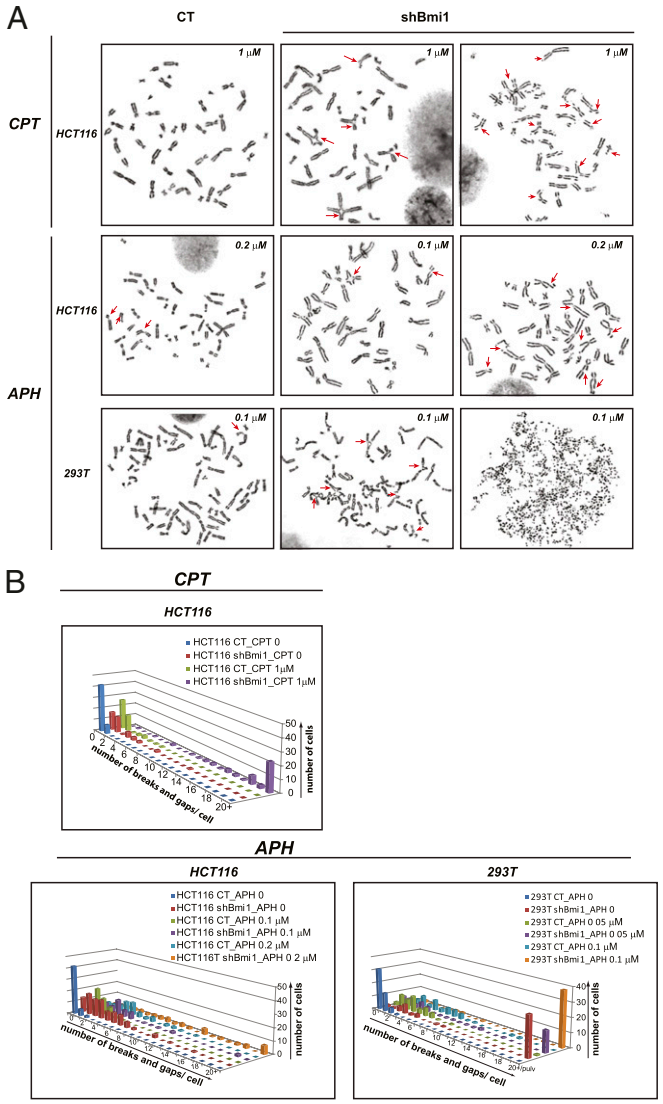

Fig. 2. Cells with reduced levels of BMI1 are highly susceptible to clastogen-induced chromosome breaks. (*A*) Control and shBmi1-tranfected HCT116 and 293T cells were exposed to APH (0.1 μM and 0.2 μM for HCT116 cells, 0.05 μM and 0.1 μM for 293T cells). (*Top*) For CPT-sensitivity experiments, control and shBmi1-transfected HCT116 cells were treated with 1 μM CPT for 1 h and allowed to recover for 24 h. (*Middle* and *Bottom*) For APH-sensitivity experiments, HCT116 and 293T cells were exposed to APH for 24 h. Representative images of metaphase spreads of each population are shown. Arrows indicate radial forms or breaks. Note that only shBmi1-transfected 293T cells exhibit pulverized metaphases. (*B*) Distribution of chromosome gaps/breaks and chromatid breaks in control (CT) and shBmi1-transfected HCT116 and 293T cells exposed as in *A* to no drug (0) or to increasing concentrations of APH. Control and shBmi1-transfected HCT116 also were exposed to 1 μM CPT as described in *A*. Note that values for untreated cells (blue and red bars) are the same as those shown in Fig. 3. Chromosomal aberrations were scored in at least 50 Giemsa-stained metaphases per condition. Results shown are from two independent experiments. Reduction of BMI1 protein levels increased the frequency of DNA damage-induced chromosomal breaks in both cell lines ($P < 0.0001$, Mann–Whitney test).

Moreover, radial chromosome forms were elevated significantly in *shBmi*-transfected cells compared with control cells, regardless of the treatment. APH treatment of 293T cells engineered to express low levels of *Bmi1* resulted in a high incidence of chromosome fragmentation and pulverization (Fig. 2*A Lower Right*). The frequency and distribution of chromosome aberrations were evaluated for each population and each condition (Fig. 2*B*). As expected, CPT treatment significantly increased the yield of chromosome breaks in control HCT116 cells, with 48% of cells showing breaks compared with 16% of cells (with a maximum of one break per cell) in the untreated population (compare blue bars and green bars, Fig. 2*B Lower Left*). *Bmi1* knockdown significantly enhanced the sensitivity of HCT116 cells to CPT treatment, with 100% of cells having breaks and a maximum of 46 breaks per cell (compare green bars and purple bars, Fig. 2*B Lower Left*). Similarly, HCT116 cells with reduced *Bmi1* levels were more susceptible to APH-induced chromosome aberrations than cells with normal *Bmi1* levels (compare light blue bars and orange bars, Fig. 2*B Center*). *Bmi1* knockdown in APH-treated 293T cells resulted in a dramatic increase in the number of breaks per cell and in the number of pulverized cells, with 76% of cells displaying more than 20 breaks per cell or pulverization (see orange bars, Fig. 2*B Lower Right*). Together these data show, in two different human cell lines, that lowering *Bmi1* levels results in a high incidence of spontaneous and clastogen-induced chromosome breaks.

Primitive *Bmi1*$^{-/-}$ Hematopoietic Cells Are Hypersentitive to Clastogenic Agents. Because transformed cell lines and primary cells may behave differently, we asked whether *Bmi1* deficiency sensitizes normal primary cells to DNA damage. First, we showed that *Bmi1*$^{-/-}$ MEF are more sensitive than wild-type cells to DNA-damaging agents (Fig. S4 *A* and *B*). We next performed an alkaline comet assay using cultured lineage marker-negative (Lin$^-$) fetal liver cells isolated from *Bmi1*$^{+/+}$ or *Bmi1*$^{-/-}$ embryos. Strikingly, cultures initiated with *Bmi1*$^{-/-}$ primitive cells generated numerous damaged cells (with comet tails) compared with control cells. The reintroduction of *Bmi1* in freshly isolated *Bmi1*$^{-/-}$ cells led to a nearly complete rescue of the DNA integrity (Fig. S4*C*).We also observed that sorted *Bmi1*$^{-/-}$ Lin$^-$Sca1$^+$ cells are more sentistive than the wild-type counterpart to CPT (Fig. S4*D*).

To determine whether *Bmi1* deficiency confers increased sensitivity to DNA damage in vivo, we exposed 6-wk-old *Bmi1*-knockout mice to whole-body irradiation. As shown in Fig. 3*A*, although none of the irradiated wild-type or heterozygote mice showed mortality, all *Bmi1*-deficient mice died within 3 wk after exposure to 500 cGy γ irradiation.

We next determined whether in vivo exposure to the ROS scavenger NAC could confer protection to *Bmi1*-deficient mice that show elevated ROS levels (Fig. 3*B* and ref. 9). This treatment, although reducing the ROS levels in *Bmi1*-deficient hematopoietic cells, failed to prevent mortality of *Bmi1*$^{-/-}$ mice after irradiation (Fig. 3*A*, gray line, and Fig. 3*B*). Moreover, histological analysis revealed that, regardless of NAC pretreatment, bone marrow from irradiated *Bmi1*$^{-/-}$ mice was severely hypoplastic and replaced by adipocytes (Fig. 3*C Lower*). Bone marrow specimens isolated from irradiated wild-type littermates were histologically normal (Fig. 3*C Upper*), indicating a complete recovery of control cells. In agreement with these results, we observed a dramatic reduction in bone marrow progenitor numbers in irradiated *Bmi1*$^{-/-}$ mice (Fig. 3*D*, red bars). Irradiation also dramatically increased the proportion of apoptotic *Bmi1*$^{-/-}$ cells compared with control cells (Fig. 3*E*).

To monitor the impact of in vivo irradiation on the proliferation of primitive *Bmi1*$^{-/-}$ bone marrow cells, we performed a CFSE dye-dilution analysis with Lin$^-$ cells (mutant and controls) over a 3-d period (Fig. 3*F Upper*). Under these conditions, nonirradiated Lin$^-$ wild-type cells underwent multiple rounds of division after a 72-h culture (Fig. 3*Fa*). Lin$^-$ cells derived from cultures initiated with *Bmi1*$^{-/-}$ bone marrow cells exhibited a much higher proportion of early-generation cells (CFSE^{high}) compared with the wild-type counterpart, pointing to a proliferation defect (Fig. 3*Fc*). After 2-Gy exposure, the wild-type cell population showed significant recovery, because most of Lin$^-$ cells resumed cycling and had progressed through approximately five divisions by 72 h (Fig. 3*Fb*). In contrast, the majority of Lin$^-$ *Bmi1*$^{-/-}$ irradiated cells were permanently arrested after one di-

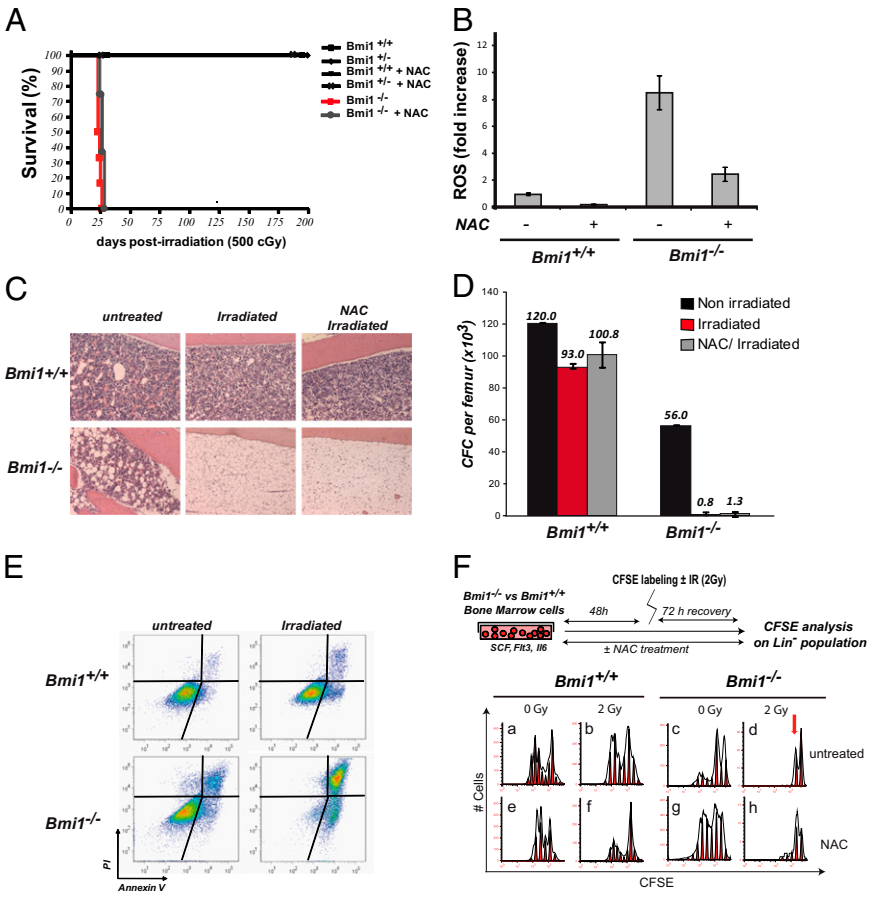

Fig. 3. Radiation sensitivity of *Bmi1*-knockout mice. (*A*) Survival curves of 6-wk-old Bmi1-knockout ($n = 6$), heterozygotes ($n = 6$), and wild-type ($n = 6$) mice subjected to 500 cGy of whole-body γ irradiation. In selected experiments, animals ($n = 3$ per genotype) were treated with NAC (1 mg/mL) given in drinking water 1 wk before irradiation. Although wild-type and heterozygotes animals survived, all *Bmi1*-knockout mice died within 3 wk of irradiation, regardless of NAC pretreatment ($P = 0.0001$). (*B*) Bone marrow cells isolated from from 6-wk-old Bmi1$^{+/+}$ and Bmi1$^{-/-}$ mice pretreated or not with NAC as described in *A*, were assayed for intracellular ROS levels using carboxyfluorescein diacetate (CFDA) staining. Results show means ± SD of results in three individual mice. (*C*) Representative histological sections of H&E-stained femurs isolated from nonirradiated or irradiated animals, pretreated or not with NAC. For comparison, age-matched control (*Bmi1*$^{+/+}$) mice (*Upper*) were killed and examined in parallel with *Bmi1*$^{-/-}$ moribund animals (*Lower*). (*D*) Bone marrow cells isolated from nonirradiated or irradiated animals, pretreated or not with NAC, were assayed for their content in colony-forming cells (CFC). Results show means ± SD of results in three individual mice. (*E*) Bone marrow cells from nonirradiated or irradiated animals, pretreated or not with NAC, were collected and subjected to apoptosis assay. The proportion of apoptotic cells was monitored by annexin V/propidium iodide staining. FACS profiles are representatives from three independent experiments. (*F*) Bone marrow cells from 6-wk-old Bmi1$^{+/+}$ and Bmi1$^{-/-}$ mice were cultured for 5 d in the presence or absence of NAC (100 μM). At day 2 of the culture, cells were labeled with CFSE and were exposed or not exposed to 2 Gy γ irradiation. Lin^{-}-gated populations were analyzed by FACS for CFSE content at 72 h postlabeling.

vision (arrow in Fig. 3*Fd*). Again, NAC pretreatment was largely ineffective in preventing this effect (Fig. 3*Fh*). These data clearly show that ROS scavenging failed to prevent DNA damage-induced cell-cycle arrest in *Bmi1*$^{-/-}$ primitive hematopoietic cells.

Bmi1 Is Required For Efficient Transcriptional Repression at Damaged Foci. Because elevated ROS levels could not account completely for the DNA damage checkpoint defects observed in knockout cells, we next delineated the precise role of BMI1 in the established DNA damage-signaling cascade.

As recently shown by others (11, 13), we first confirmed that BMI1 is recruited rapidly to DNA damage foci after exposure to UV light (Fig. S5), γ irradiation (Fig. S6 *A*–*C*), and S phase-specific genotoxic agents such as CPT and hydroxyurea (HU) (Fig. S6*A*). This recruitment is observed in both HeLa and HCT116 cell lines (Figs. S5 and S6 *D* and *E*) and in primary cells (MEF and primitive hematopoietic cells) (Fig. S6 *A*–*C*). Moreover, coimmunoprecipitation experiments performed with HCT116 cell extracts showed that endogenous BMI1 associates with γ-H2AX and mono- and diubiquitin γ-H2AX at the chromatin-bound fraction upon irradiation (Fig. S6*F*).

Considering the role of PcG proteins in gene silencing, we next investigated whether BMI1 accumulated to DNA damage foci to repress transcriptional activity at the injured site. RNA polymerase II (pol II)-mediated transcriptional elongation is associated with extensive phosphorylation at the serine 2 (ser2) residue (24). We examined the presence of RNA pol II (ser2) phosphorylation at γ-H2AX^{+} foci following UV treatment in *Bmi1*$^{+/+}$ and *Bmi1*$^{-/-}$ MEF. As shown in Fig. 4*A*, although RNA pol II (ser2) was excluded consistently from DSB after UV exposure in wild-type cells, it clearly colocalized with γ-H2AX–induced foci in *Bmi1*$^{-/-}$ cells (compare enlarged images in WT versus knockout-derived cells in Fig. 4*A*). Image-based quantification indicated a 5 ± 0.8-fold increase in RNA pol II (ser2) mean fluorescence intensity at γ-H2AX^{+} foci in *Bmi1*$^{-/-}$ cells (Fig. 4*B*).

Defect in Homologous Recombination in Cells Expressing Low Levels of *Bmi1*. We next tested whether *Bmi1*-deficient cells have a bona fide homologous recombination (HR) defect using the HR reporter assay system established by Jasin and coworkers (25) as depicted in Fig. 5*A*. In this system, cleavage of the I-SceI site between two incomplete EGFP genes (SceGFP and iGFP)

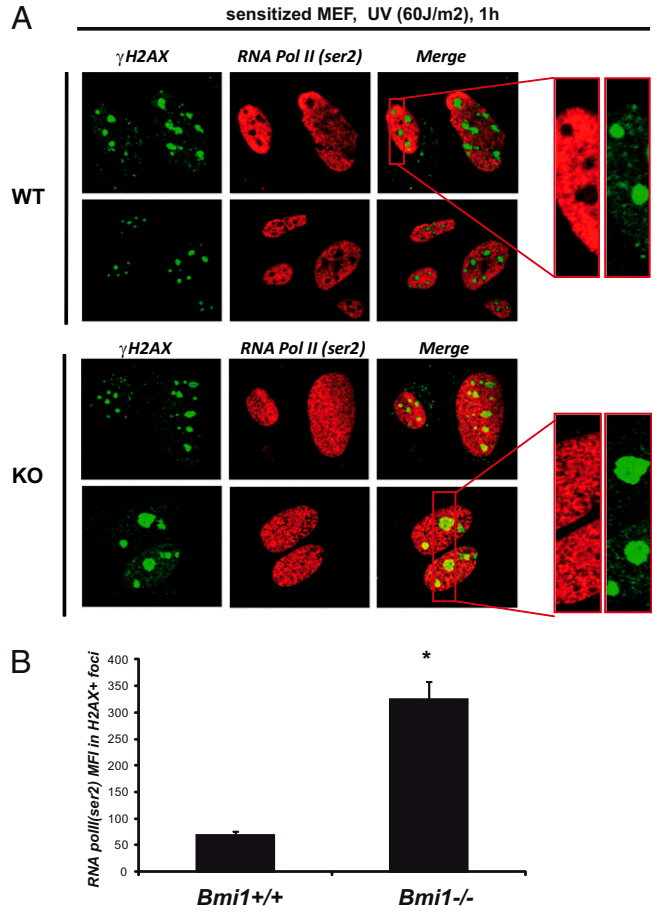

Fig. 4. BMI1 is required for transcriptional repression at DNA lesions. (*A*) *Bmi1*$^{+/+}$ (WT) and *Bmi1*$^{-/-}$ (KO) MEF were sensitized with 2 μg/mL Hoechst 33258 for 15 min before exposure to 60 J/m^2 UV light and were allowed to recover for 1 h. Cells then were immunostained for γ-H2AX (green) and phosphorylated (ser2) RNA pol II (red). Images show two fields from two independent experiments. (*B*) Image-based analysis using the Operetta system (PerkinElmer) for quantification of RNA pol II (ser2) in γ-H2AX$^+$ spots. *$P < 0.005$, Student *t* test.

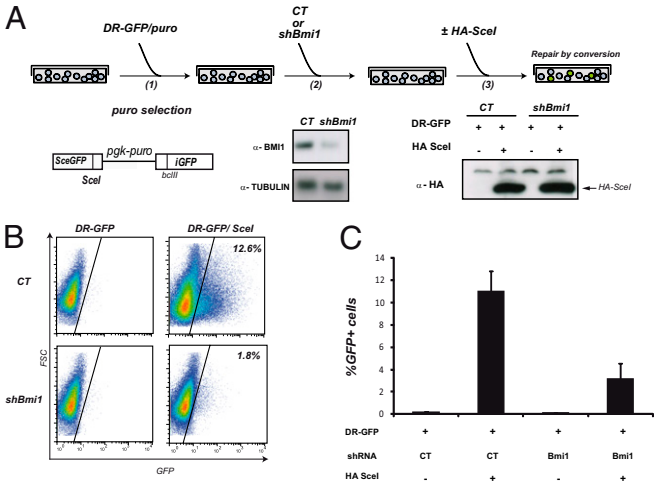

Fig. 5. Bmi1 is required for efficient DNA repair. (*A*) 293T cells were transfected first with the HR reporter DR-GFP and selected for 2 d with puromycin (2 μg/mL). Cells expressing DR-GFP were transfected further with a control (CT) or an shBmi1 vector and kept in culture for 1 d. Finally, cells were transfected with an I-SceI expression vector, harvested after 36 h, and subjected to flow cytometry analysis to determine percentages of GFP$^+$ cells resulting from gene conversion repair. (*B*) Representative FACS profiles from one of three independent experiments. (C) Percentages of GFP$^+$ cells as assessed by flow cytometry 36 h after I-SceI transfection. Results show mean ± SD of three independent experiments.

induces HR, thereby resulting in the restoration of a functional GFP gene. Fig. 5*B* shows a typical example of GFP expression level in control cells (*Upper Right*) and *shBmi1*-transfected cells (*Lower Right*) following ectopic expression of SceI endonuclease. As summarized in Fig. 5*C*, the proportion of GFP$^+$ cells falls from 11 ± 1.9% in control cells to 3.2 ± 1.3% in cells expressing an shRNA vector to *Bmi1*, thus supporting its contribution in HR-dependent DNA repair.

Discussion

The ability to maintain genome integrity has emerged as a critical influence on stem cell longevity (26). This capacity relies on the proper execution of a finely tuned molecular network that coordinates DNA repair with cell-cycle progression. In the present study, we uncovered a function for *Bmi1* in safeguarding chromosomal integrity of primitive hematopoietic cells and of transformed/immortalized cell lines. Moreover, our results reinforced recent observations documenting a delocalization of BMI1 at DNA lesions upon DNA damage (11–13).

During the course of our study, another group reported the recruitment of multiple members of PcG complexes (PRC1 and PRC2) to DSB. This recruitment occurs independently of ataxia telangiectasia-mutated (ATM) and ataxia telangiectasia and Rad3-related (ATR) kinases (11). Interestingly, BMI1 recruitment to DSB required its really interesting new gene (RING) domain as well as the fork-head–associated (FHA) and breast cancer gene 1 C-terminal (BRCT) domains of nibrin (NBS1) (13) and occurs in a PARP1/2-dependant manner (11).

Our study also demonstrates that loss of *Bmi1* does not prevent or delay the DNA damage-induced formation of γ-H2AX foci, indicating that *Bmi1* is dispensable for the initial recognition of DNA breaks.

Considering these observations, one could ask whether BMI1 is recruited to repress transcription of genes located in the damaged area and/or is involved in posttranslational modifications that allow the sequential accrual of many DNA damage/repair proteins.

Strikingly, we observed an aberrant RNA pol II (ser2) phosphorylation, a mark that denotes transcription elongation, at DSBs, strongly suggesting a role for BMI1 in transcriptional repression of the damaged area.

Interestingly, the persistent γ-H2AX foci observed in *Bmi1*-deficient cells were larger than those detected in wild-type cells. Two main classes of DNA damage-induced foci have been described: the early, small foci that are observed from 10 min to 8 h after induction of DNA damage, and the late, larger foci that appear only after 4 h following DNA damage and persist after the majority of breaks have been repaired. It has been suggested that these late foci mark the location of lesions that are particularly difficult to repair (27, 28). Thus, it is conceivable that loss of *Bmi1* impedes the repair of late DNA damage-induced foci. Consistent with a persistence of unrepaired damage and a checkpoint recovery defect, *Bmi1* depletion leads to a hyperactivated and sustained ATM/checkpoint kinase 2 (CHK2) pathway (19), raising the possibility that *Bmi1*-deficient HSCs undergo premature senescence as a result of accumulated DNA damage.

Supporting a role for PRC1 in protein ubiquitination, loss of *Bmi1* dramatically diminishes the accumulation of ubiquitin conjugates (including ubiquitin–γ-H2AX) upon DNA damage (13) and hence impinges on the subsequent signal amplification that is indispensable for efficient repair.

p53 and retinoblastoma (Rb) proteins are known to play a critical role in the maintenance of the G2 checkpoint and in the prevention of mitotic catastrophes in response to DNA damage

occurring between the S and G2 phases (29). In fact, abrogation of the G2 checkpoint in p53-deficient HCT116 cells results in chromosome fragmentation in response to APH-induced DNA damage (30). Therefore, the chromosome pulverization observed in p53-deficient 293T cells (31) may result from the combination of *Bmi1* depletion and impaired G2 checkpoint. Importantly, we also found that *Bmi1* deficiency sensitizes MEF and primary hematopoietic cells to clastogenic agents.

Several inherited bone marrow failure syndromes leading to aplastic anemia, such as dyskeratosis congenita or Fanconi anemia, are regarded as genomic instability disorders (32). Here we show that, in addition to the aplastic anemia and HSC exhaustion previously described, *Bmi1*-deficient cells share several features with genomic instability disorders, including accumulation at the G2/M phase of the cell cycle and chromosome instability. The absence of mitotic cells in splenocytes isolated from *Bmi1*-deficient mice precludes the analysis of chromosomal instability as classically performed. However, cytogenetic analysis performed on two different cell lines clearly showed that reduction in BMI1 protein levels results in an increase in spontaneous chromosome aberrations and hypersensitivity to DNA-damaging agents. The presence of radial chromosome structures in cells with reduced BMI1 levels further emphasizes the similarities with genomic instability disorders.

Overgeneration of ROS has been prominently associated with genomic instability and premature aging phenotypes. Considering the recent role ascribed to *Bmi1* in antioxidative defense mechanisms (18), one could ask whether the acute radiation sensitivity of *Bmi1*-deficient mice might arise from the elevated ROS levels. Furthermore, recent studies revealed an unsuspected role for oxidative metabolism in the regulation of hematopoietic cell fate, because the induction of ROS production in *Drosophila* led to premature differentiation of all blood cells (33). Taken together, these observations raised the possibility that PcG-mediated function in HSC self-renewal occurs in part through the control of ROS generation. In the present study, we confirmed that *Bmi1* deficiency leads to enhanced ROS production in hematopoietic cells. However, although antioxidant agents significantly reduced ROS levels and gave a minor proliferative advantage to $Bmi1^{-/-}$ progenitors, they failed to prevent the hypersensitivity of these cells to DNA damage. Importantly, the alteration of mitochondrial function and the ensuing enhanced ROS production observed in *Bmi1*-deficient cells occurs independently of the Ink4a/Arf pathway. Moreover, the abrogation of the abnormally activated DNA-damage response observed in *Bmi1*-deficient cells, through *chk2* deletion, although rescuing some defects of *Bmi1*-deficient mice, failed to restore the long-term repopulating ability of $Bmi1^{-/-}$ HSC (19).

Together, the results presented here document an anticlastogenic function for *Bmi1*, further expanding its involvement in multiple cellular processes and possibly explaining its key function in many different types of stem cells.

Materials and Methods

Scoring Technique Used tor Analysis of Chromosome Breakage. Analysis was performed on 50 Giemsa-stained metaphases in treated and untreated cultures for the control vector and *shBmi1*-transfected specimens. The number and type of structural chromosome abnormalities were scored. Chromatid gaps were not included in the final score. Isochromatid gaps, chromatid and isochromatid breaks, deletions, and fragments were scored as a single break. Structural rearrangements including dicentrics, rings, translocations, and radial figures were scored as two breakage events. Pulverized cells were noted. The total chromosome aberrations and the average number of aberrations per cell were scored for each sample. Dicentrics and translocations were not scored for the aphidicolin test using the 293T transfected cells.

ACKNOWLEDGMENTS. We thank Sylvie Lavallée for her expertise and help with cytogenetic analysis, Valeria Azcoitia for help with histology, Melanie Fréchette for help in maintaining and manipulating the animals, and Danièle Gagné for assistance with flow cytometry. This work was supported by grants from the Canadial Institutes of Health Research (to G.S.) and from Fonds de la Recherche en Santé du Québec (Cancer Research Network) (to J.H.) J.C. is a Fellow of the American Society of Hematology, and G.S. is a recipient of a Canada Research Chair in molecular genetics of stem cells.

1. Bruggeman SW, et al. (2005) Ink4a and Arf differentially affect cell proliferation and neural stem cell self-renewal in Bmi1-deficient mice. *Genes Dev* 19:1438–1443.
2. Jacobs JJ, Kieboom K, Marino S, DePinho RA, van Lohuizen M (1999) The oncogene and Polycomb-group gene Bmi-1 regulates cell proliferation and senescence through the ink4a locus. *Nature* 397:164–168.
3. Itahana K, et al. (2003) Control of the replicative life span of human fibroblasts by p16 and the polycomb protein Bmi-1. *Mol Cell Biol* 23:389–401.
4. Oguro H, et al. (2006) Differential impact of Ink4a and Arf on hematopoietic stem cells and their bone marrow microenvironment in Bmi1-deficient mice. *J Exp Med* 203:2247–2253.
5. Bracken AP, et al. (2007) The Polycomb group proteins bind throughout the INK4A-ARF locus and are disassociated in senescent cells. *Genes Dev* 21:525–530.
6. Kotake Y, et al. (2007) pRB family proteins are required for H3K27 trimethylation and Polycomb repression complexes binding to and silencing p16INK4alpha tumor suppressor gene. *Genes Dev* 21:49–54.
7. Lessard J, Sauvageau G (2003) Bmi-1 determines the proliferative capacity of normal and leukaemic stem cells. *Nature* 423:255–260.
8. Le Cam L, et al. (2006) E4F1 is an atypical ubiquitin ligase that modulates p53 effector functions independently of degradation. *Cell* 127:775–788.
9. Chagraoui J, et al. (2006) E4F1: A novel candidate factor for mediating BMI1 function in primitive hematopoietic cells. *Genes Dev* 20:2110–2120.
10. Cao R, Tsukada Y, Zhang Y (2005) Role of Bmi-1 and Ring1A in H2A ubiquitylation and Hox gene silencing. *Mol Cell* 20:845–854.
11. Chou DM, et al. (2010) A chromatin localization screen reveals poly (ADP ribose)-regulated recruitment of the repressive polycomb and NuRD complexes to sites of DNA damage. *Proc Natl Acad Sci USA* 107:18475–18480.
12. Facchino S, Abdouh M, Chatoo W, Bernier G (2010) BMI1 confers radioresistance to normal and cancerous neural stem cells through recruitment of the DNA damage response machinery. *J Neurosci* 30:10096–10111.
13. Ismail IH, Andrin C, McDonald D, Hendzel MJ (2010) BMI1-mediated histone ubiquitylation promotes DNA double-strand break repair. *J Cell Biol* 191:45–60.
14. Hong Z, et al. (2008) A polycomb group protein, PHF1, is involved in the response to DNA double-strand breaks in human cell. *Nucleic Acids Res* 36:2939–2947.
15. Rouleau M, et al. (2007) PARP-3 associates with polycomb group bodies and with components of the DNA damage repair machinery. *J Cell Biochem* 100:385–401.
16. Bergink S, et al. (2006) DNA damage triggers nucleotide excision repair-dependent monoubiquitylation of histone H2A. *Genes Dev* 20:1343–1352.
17. Klein UR, Nigg EA (2009) SUMO-dependent regulation of centrin-2. *J Cell Sci* 122:3312–3321.
18. Chatoo W, et al. (2009) The polycomb group gene Bmi1 regulates antioxidant defenses in neurons by repressing p53 pro-oxidant activity. *J Neurosci* 29:529–542.
19. Liu J, et al. (2009) Bmi1 regulates mitochondrial function and the DNA damage response pathway. *Nature* 459:387–392.
20. van der Lugt NM, et al. (1994) Posterior transformation, neurological abnormalities, and severe hematopoietic defects in mice with a targeted deletion of the bmi-1 proto-oncogene. *Genes Dev* 8:757–769.
21. Benveniste P, et al. (2010) Intermediate-term hematopoietic stem cells with extended but time-limited reconstitution potential. *Cell Stem Cell* 6:48–58.
22. Jacobs JJ, et al. (2000) Senescence bypass screen identifies TBX2, which represses Cdkn2a (p19(ARF)) and is amplified in a subset of human breast cancers. *Nat Genet* 26:291–299.
23. Bowie MB, Kent DG, Copley MR, Eaves CJ (2007) Steel factor responsiveness regulates the high self-renewal phenotype of fetal hematopoietic stem cells. *Blood* 109:5043–5048.
24. Komarnitsky P, Cho EJ, Buratowski S (2000) Different phosphorylated forms of RNA polymerase II and associated mRNA processing factors during transcription. *Genes Dev* 14: 2452–2460.
25. Johnson RD, Liu N, Jasin M (1999) Mammalian XRCC2 promotes the repair of DNA double-strand breaks by homologous recombination. *Nature* 401:397–399.
26. Rossi DJ, et al. (2007) Deficiencies in DNA damage repair limit the function of haematopoietic stem cells with age. *Nature* 447:725–729.
27. Maser RS, Monsen KJ, Nelms BE, Petrini JH (1997) hMre11 and hRad50 nuclear foci are induced during the normal cellular response to DNA double-strand breaks. *Mol Cell Biol* 17:6087–6096.
28. Nelms BE, Maser RS, MacKay JF, Lagally MG, Petrini JH (1998) In situ visualization of DNA double-strand break repair in human fibroblasts. *Science* 280:590–592.
29. Flatt PM, Tang LJ, Scatena CD, Szak ST, Pietenpol JA (2000) p53 regulation of G(2) checkpoint is retinoblastoma protein dependent. *Mol Cell Biol* 20:4210–4223.
30. Nitta M, et al. (2004) Spindle checkpoint function is required for mitotic catastrophe induced by DNA-damaging agents. *Oncogene* 23:6548–6558.
31. Bargonetti J, Reynisdóttir I, Friedman PN, Prives C (1992) Site-specific binding of wild-type p53 to cellular DNA is inhibited by SV40 T antigen and mutant p53. *Genes Dev* 6: 1886–1898.
32. Dokal I, Vulliamy T (2008) Inherited aplastic anaemias/bone marrow failure syndromes. *Blood Rev* 22:141–153.
33. Owusu-Ansah E, Banerjee U (2009) Reactive oxygen species prime Drosophila haematopoietic progenitors for differentiation. *Nature* 461:537–541.